

Mechanical response of bovine articular cartilage under dynamic unconfined compression loading at physiological stress levels

S. Park M.S., C. T. Hung Ph.D. and G. A. Ateshian Ph.D.*

Columbia University, Departments of Mechanical Engineering and Biomedical Engineering,
New York, NY, USA

Summary

Objective: The objective of this study was to characterize the dynamic modulus and compressive strain magnitudes of bovine articular cartilage at physiological compressive stress levels and loading frequencies.

Design: Twelve distal femoral cartilage plugs (3 mm in diameter) were loaded in a custom apparatus under load control, with a load amplitude up to 40 N and loading frequencies of 0.1, 1, 10 and 40 Hz, resulting in peak Cauchy stress amplitudes of 4.8 MPa (engineering stress 5.7 MPa).

Results: The equilibrium Young's modulus under a tare load of 0.4 N was 0.49 ± 0.10 MPa. In the limit of zero applied stress, the incremental dynamic modulus derived from the slope of the stress–strain curve increased from 14.6 ± 6.9 MPa at 0.1 Hz to 28.7 ± 7.8 MPa at 40 Hz. At 4 MPa of applied stress, the corresponding increase was from 48.2 ± 13.5 MPa at 0.1 Hz to 64.8 ± 13.0 MPa at 40 Hz. Peak compressive strain amplitudes varied from $15.8 \pm 3.4\%$ at 0.1 Hz to $8.7 \pm 1.8\%$ at 40 Hz. The phase angle decreased from $28.8^\circ \pm 6.7^\circ$ at 0.1 Hz to $-0.5^\circ \pm 3.8^\circ$ at 40 Hz.

Discussion: These results are representative of the functional properties of articular cartilage under physiological load magnitudes and frequencies. The viscoelasticity and nonlinearity of the tissue helps to maintain the compressive strains below 20% under the physiological compressive stresses achieved in this study. These findings have implications for our understanding of cartilage metabolism and chondrocyte viability under various loading regimes. They also help establish guidelines for cartilage functional tissue engineering studies. © 2003 OsteoArthritis Research Society International. Published by Elsevier Ltd. All rights reserved.

Key words: Cartilage mechanics, Unconfined compression, Dynamic loading, Physiological stress levels.

Introduction

One of the unresolved questions in articular cartilage biomechanics is the magnitude of tissue compressive strains under physiological loading conditions. While load magnitudes in various diarthrodial joints have been estimated with reasonable confidence for a number of activities of daily living^{1–4}, and while articular contact stresses have been measured with good accuracy under such load magnitudes in a number of studies^{5–10}, there are only a few reports of measurements of cartilage deformation under physiological conditions. Armstrong *et al.*¹¹ reported compressive strains of up to 20% under physiological loads in human cadaveric hip joints, using a radiographic technique; Macirowski *et al.*¹² demonstrated changes in cartilage thickness on the order of 10% or less using ultrasound measurements; in their *in vivo* study using magnetic resonance imaging, Eckstein *et al.*^{13,14} reported a decrease of approximately 3% in cartilage thickness following 30 deep knee bends, while the cadaveric study by Herberhold *et al.*¹⁵ showed a progressive decrease in cartilage thickness over 4 h by 57% under a constant load. In a rabbit

model, Kaab *et al.*¹⁶ reported reductions in cartilage thickness of 46% under static loading and 22–34% under dynamic loading, when compared to unloaded controls.

Knowledge of the physiological level of strain magnitudes is essential for our understanding of articular cartilage metabolism (catabolic and anabolic activities) in response to physical loading and chondrocyte mechanotransduction. Many basic science studies have investigated the response of cartilage explants^{17–23} or chondrocyte-seeded scaffolds^{24–27} to various compressive loading conditions. In these studies, determination of whether or not the loading environment falls within physiologic bounds would facilitate interpretation of the results. Similarly, studies which attempt to provide a physiological loading environment for promoting functional mechanical properties in tissue engineered cartilage^{28–32} may benefit from a more accurate assessment of the compressive strain and stiffness of native cartilage under physiological conditions.

The magnitude of contact stresses in natural joints under light to moderate activities typically ranges from 1 to 6 MPa^{5,6}; under more strenuous activities, peak contact stresses in natural joints have been estimated in the range of 12 MPa⁹; and in a classical study by Hodge *et al.*⁸, the contact stress measured *in vivo* using an instrumented hip endoprosthesis was found to reach 18 MPa while rising from a chair. These contact stresses are always compressive and it may seem straightforward to estimate strain magnitudes by dividing these stress values with the

*Address correspondence and reprint requests to: G. A. Ateshian, Departments of Mechanical Engineering and Biomedical Engineering, Columbia University, 500 West 120th St, MC4703, 220 S.W. Mudd, New York, NY 10027, USA. Tel: 212-854-8602, Fax: 212-854-3304; E-mail: ateshian@columbia.edu

Received 10 September 2002; revision accepted 8 August 2003.

compressive modulus of articular cartilage reported in the literature. However, this estimation is significantly complicated by the viscoelastic and nonlinear response of cartilage to loading. The equilibrium confined compression (aggregate) or unconfined compression (Young's) modulus of articular cartilage, which is on the order of 0.5 MPa³³ even up to 50% compression³⁴, is clearly too low to obtain a plausible estimate of compressive strain under physiological loading, since using this compressive modulus within a simplistic linear analysis would predict that cartilage is effectively crushed when compressive stresses exceed ~2 MPa. However, it has been recognized that the equilibrium response of articular cartilage, though easily achieved under laboratory conditions, is not physiological because it occurs only after several hours of static loading, when cartilage interstitial fluid has exuded from the tissue and the interstitial fluid pressure has reduced to zero^{35–37}. Under cyclical loading at physiological frequencies (e.g., 0.01–2 Hz), the interstitial fluid pressure of cartilage is maintained at elevated values^{38–40} and the tissue's dynamic modulus is considerably higher than the equilibrium modulus^{18,21,39,41}. In unconfined compression cyclical loading, the dynamic modulus of bovine articular cartilage at 1 Hz has been measured at 13, 20, and 37 MPa under strain amplitudes of 0.5, 1, and 2.5%, respectively^{18,21,41}; despite the fact that these results were reported in different studies, they strongly suggest that the dynamic response of cartilage in unconfined compression is nonlinear with respect to compressive strain. It can be estimated from these results that the compressive stresses achieved in these studies (whose purpose was to characterize cartilage properties under small strains, not necessarily under physiological compressive stresses) were on average less than 1 MPa. Since the majority of dynamic loading studies of articular cartilage have been conducted under displacement control (where the compressive strain is prescribed), whereas the physiological loading environment has been primarily characterized under load control (by measuring contact stresses in cadaveric joints under physiological load magnitudes), the specific objective of the present study was to perform unconfined compression cyclical loading tests on bovine articular cartilage under load control, with applied 'engineering' stresses nominally in the range of 0 to ~5.7 MPa and loading frequencies in the range 0.1–40 Hz, to characterize the mechanical response of this tissue to physiological load magnitudes.

Materials and methods

Twelve cylindrical cartilage plugs, 3 mm in diameter, were harvested from the trochlea and condyles of the distal femoral articular layer of four fresh frozen bovine knee joints (3 months to 3 years old) obtained from a local abattoir. Using a sledge microtome (Model 1400; Leiz, Rockleigh, NJ), approximately 0.5 mm of tissue was removed from the deep zone to remove remnants of subchondral bone and vascularized tissue and to produce a surface parallel to the articular side, leaving the articular surface intact. The harvested samples (thickness $h=1.83\pm 0.15$ mm) were then stored at -25°C until ready for use. The testing apparatus (Fig. 1), custom-designed for this study, consisted of a voice-coil force actuator (Model LA17-28-000A; BEI Kimco Magnetics Division, San Marcos, CA, 71 N peak force), connected in series with a linear variable differential transformer (LVDT) for displacement measurements (Model PR812-200, Schaeviz

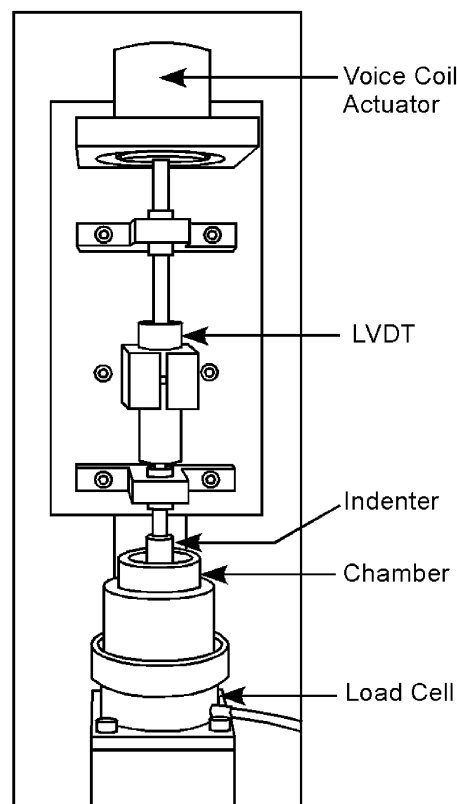


Fig. 1. Schematic of the custom-designed testing apparatus.

Sensors, Hamptons, VA, ± 5 mm), a loading platen consisting of 1 mm thick glass, the tissue sample, and a stainless steel specimen chamber mounted on a load cell (Model 8523, Burster, Sterling Heights, MI, ± 200 N). The voice-coil force actuator, connected to a power supply (Model PST-040-13-DP, Copley Controls Corp., Canton, MA, +40VDC at 13 A continuous) and controller box (Model TA115, Trust Automation Inc., San Luis Obispo, CA, 150 W continuous/325 W peak) was controlled via a force feedback loop using a desktop computer (Intel Pentium 4 CPU) with a data input and output board (Model PCI-MIO-16XE-10, National Instruments, Austin, TX) running the LabView software package (Version 5.0, National Instruments, Austin, TX). Low-pass filters (with a cutoff frequency of 85 or 231 Hz depending on the frequency of the applied load) were used to reduce noise from the load cell and LVDT. In the absence of a test sample, under a tare load of 1 N and a dynamic load amplitude of 7 N, the device yielded a dynamic stiffness of 0.72 ± 0.05 N/ μm (range 0.65–0.78 N/ μm) and phase angle of $0.1\pm 0.5^{\circ}$ (range -0.3 – 0.8°) in the frequency range 0.1–40 Hz. This system compliance was accounted for in all measurements of test samples. Furthermore, it was shown that the dynamic modulus and phase angle of a cylindrical rubber specimen (1.70 mm thick, ϕ 6 mm) under a 4 N load amplitude varied from 3.11 ± 0.05 MPa and $3.77^{\circ}\pm 1.10^{\circ}$ at 0.1 Hz to 3.60 ± 0.19 MPa and $1.32^{\circ}\pm 4.37^{\circ}$ at 40 Hz ($n=3$ repeated measures).

On the day of testing, specimens were thawed at room temperature in normal phosphate buffered saline (PBS) solution for 1 h and the thickness was measured with a

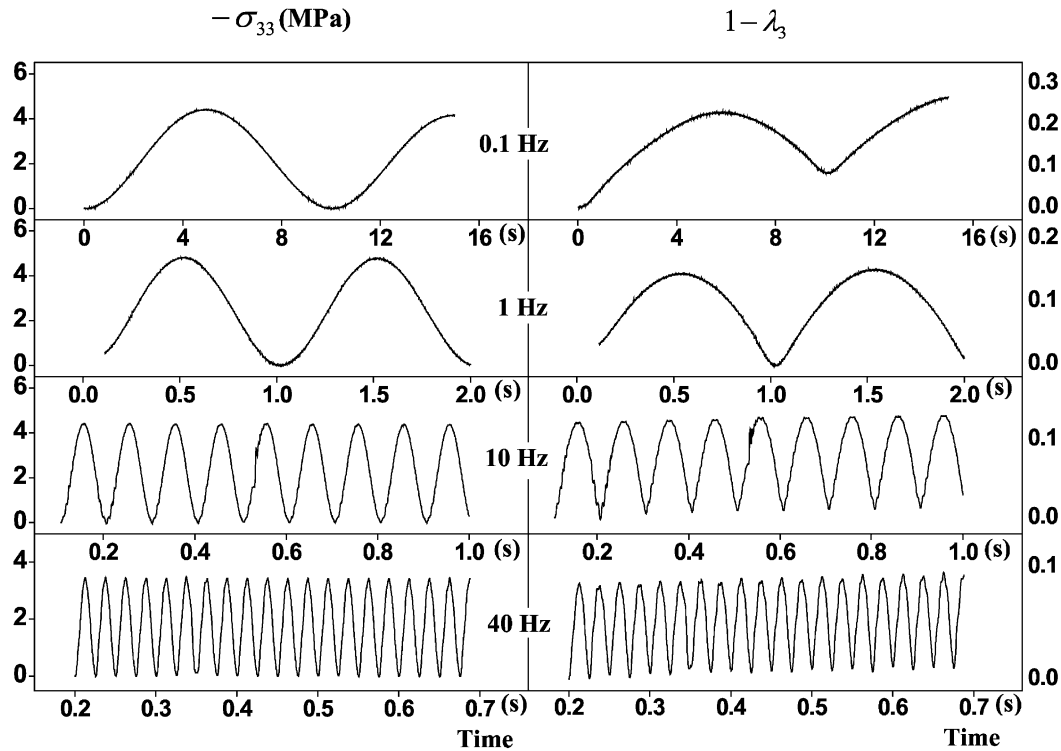


Fig. 2. Stress vs time and strain vs time for a typical specimen at various loading frequencies.

custom micrometer device. All subsequent tests were performed in PBS. To zero the position of the loading platens, the specimen was mounted on the device and the platen was lowered until a small load less than 0.1 N was registered; this load was removed in less than a minute. A tare load of 0.4 N (equivalent to 57 kPa) was then applied onto each sample to maintain proper loading platen contact, and the specimen was allowed to equilibrate under this tare load (1.5 h). The reduction in thickness resulting from tare load application was $12.0 \pm 2.3\%$ of the original sample height, as measured from the zeroed loading platen position, and an equilibrium Young's modulus was determined from these measurements. Cyclical compressive loads were then applied onto the specimen using a sinusoidal profile of the form $F = F_0(1 - \cos 2\pi ft)/2$ (where f is the loading frequency), nominally varying in amplitude from 0 to $F_0 = 40$ N (equivalent to 'engineering' stresses in the range 0–5.7 MPa when calculated with the initial surface area of the specimen) above the initial tare load. This choice of loading profile was motivated by the desire to guarantee a full sinusoidal loading profile with no loading platen lift-off, while keeping the tare load small. Cyclical loads consisted of 40 cycles at 40 Hz, 10 cycles at 10 Hz, two cycles at 1 Hz, and one cycle at 0.1 Hz, and were applied in that given order. Because the mean applied load was equal to $F_0/2$, the specimen dynamic deformation was accompanied by a creep deformation (Fig. 2); thus, between each set of loading frequencies, the specimen was allowed to recover for 5–30 min, in proportion to the duration of loading.

Since physiological load magnitudes may produce strains in the finite deformation range, it is necessary to clarify the method by which material properties were evaluated. The data were evaluated as Cauchy normal stress

component versus stretch ratio (σ_{33} vs λ_3 , where the three-direction denotes the axial loading direction), assuming that the response of cartilage at these tested frequencies is nearly incompressible ($\lambda_3 = h/h_0$, $\sigma_{33} = hF/h_0A_0$, where F is the applied load, h the sample thickness in the deformed configuration, and h_0 , A_0 are the thickness and cross-sectional area in the reference configuration). The mechanical response was observed to be nonlinear, which precluded the use of standard Fourier transform analysis commonly used for linear responses under small strains^{18,21,41}. To capture the nonlinearity of the response, the time-varying data at each loading frequency were plotted as stress vs strain (σ_{33} vs $\lambda_3 - 1$) and the data corresponding to the loading phase (i.e., when the compressive stress is increasing during the loading cycle) were fitted with a suitable function for the purpose of smoothing. The slope of this function ($\partial\sigma_{33}/\partial\lambda_3$) was then evaluated to provide the incremental dynamic modulus as a function of compressive strain (or stress), at that given frequency. According to standard continuum mechanics relations valid under finite deformation⁴², the energy W stored or dissipated during loading of a cylindrical specimen is given by the integral of σ_{33}/λ_3 over the corresponding range of λ_3 , under the same assumption of incompressibility used above¹. If we denote this integral by W_l during the loading phase, and W_u during the unloading phase of one complete cycle, the phase angle δ can then be evaluated from $\tan \delta = 4(W_l + W_u)/\pi(W_l - W_u)$.

¹ This expression is valid for isotropic, cubic, transversely isotropic and special cases of orthotropic materials, as long as the loading direction properly coincides with one of the directions of material texture.

Table I
Mean and standard deviation of the range (Δ) of compressive stress and range of compressive strain over the loading cycles, as a function of loading frequency

Frequency (Hz)	$\Delta\sigma_{33}$ (MPa)	$\Delta(\lambda_3-1)$
0.1	-4.53 ± 0.25	-0.158 ± 0.034
1	-4.79 ± 0.16	-0.127 ± 0.023
10	-4.44 ± 0.14	-0.103 ± 0.017
40	-3.83 ± 0.52	-0.087 ± 0.018

Results

The equilibrium Young's modulus evaluated from the tare load application was measured at $E_Y=0.49\pm 0.10$ MPa. The dynamic response from a typical specimen is shown in the time domain in Fig. 2. The amplitudes of the actual applied stress and the measured strain are summarized as a function of frequency in Table I. Due to the frequency characteristics of the loading device, the applied load amplitude could be maintained at the prescribed value at the lower frequencies (39.99 ± 0.10 N at 0.1 Hz and 39.71 ± 0.09 N at 1 Hz) but decreased at the higher frequencies (35.58 ± 0.68 N at 10 Hz and 30.13 ± 4.42 N at

40 Hz). This factor, together with the fact that the stress calculations depended on the axial stretch ratio, produced a range of Cauchy stress ($\Delta\sigma_{33}$) that varied at each loading frequency (Table I). The applied load was very nearly a pure sinusoid as assessed by its total harmonic distortion (ranging from $0.03\pm 0.04\%$ at 0.1 Hz to $4.3\pm 1.5\%$ at 40 Hz).

The stress-strain responses of a typical specimen are presented in Fig. 3, at various loading frequencies, along with the corresponding curve fits. It was found that the two-parameter function $y=A(1-e^{-Bx})$ could successfully fit the σ_{33} vs λ_3-1 data at all frequencies, with the coefficients A, B and corresponding R^2 values for the curve fits provided in Table II. Differentiating these functions produces equations for the strain- or stress-dependent modulus at each loading frequency; the modulus at zero strain and the maximum modulus achieved at that particular frequency, are also presented in the table. The frequency-dependent incremental modulus is presented in Fig. 4(a) at selected compressive Cauchy stresses (0–4 MPa in increments of 1 MPa). A two-way ANOVA for the factors of loading frequency and stress show that the dynamic modulus increases significantly with applied stress at all frequencies ($P<0.0001$); frequency-dependent differences in dynamic

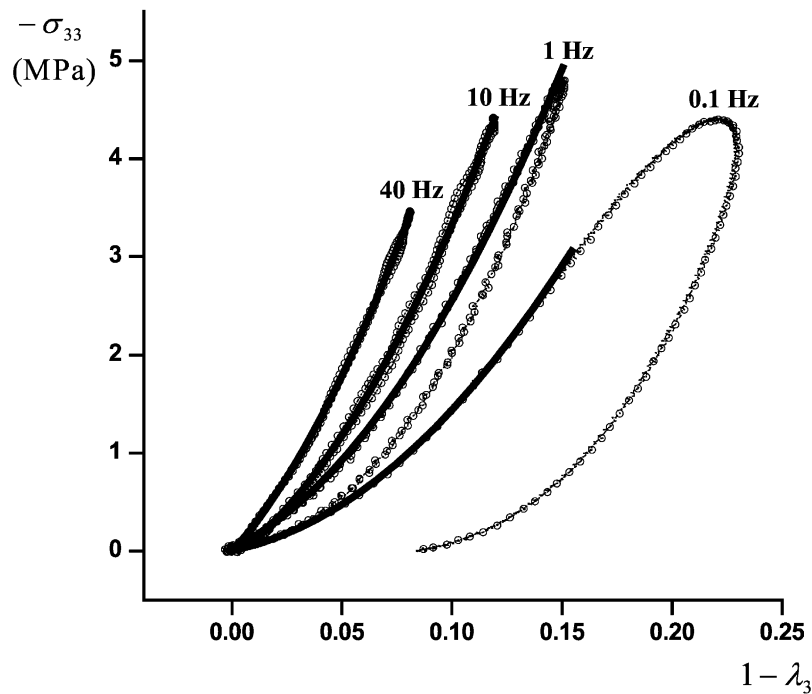


Fig. 3. Stress-strain response for a typical specimen, at various loading frequencies, and corresponding polynomial curve fits. Both σ_{33} and λ_3-1 are negative in compression.

Table II
Mean and standard deviation of the coefficients of the curve fits of the stress-strain data, $\sigma_{33}=A(1-\exp[B(1-\lambda_3)])$, and corresponding R^2 values

Frequency (Hz)	A (MPa)	B (MPa)	R^2	Minimum modulus (MPa)	Maximum modulus (MPa)
0.1	2.45 ± 2.10	8.41 ± 3.41	0.998 ± 0.001	14.6 ± 6.9	48.54 ± 17.0
1	1.59 ± 0.89	11.6 ± 3.62	0.998 ± 0.001	16.1 ± 5.2	65.7 ± 15.8
10	2.80 ± 1.21	9.49 ± 2.52	0.995 ± 0.001	24.2 ± 6.6	61.7 ± 13.3
40	3.52 ± 1.53	9.04 ± 2.72	0.993 ± 0.003	28.7 ± 7.8	60.9 ± 13.4

Minimum modulus = AB ; maximum modulus = $AB \exp[B(1-\lambda_3)]$ evaluated at the value of λ_3 where the maximum occurred, for each corresponding loading frequency.

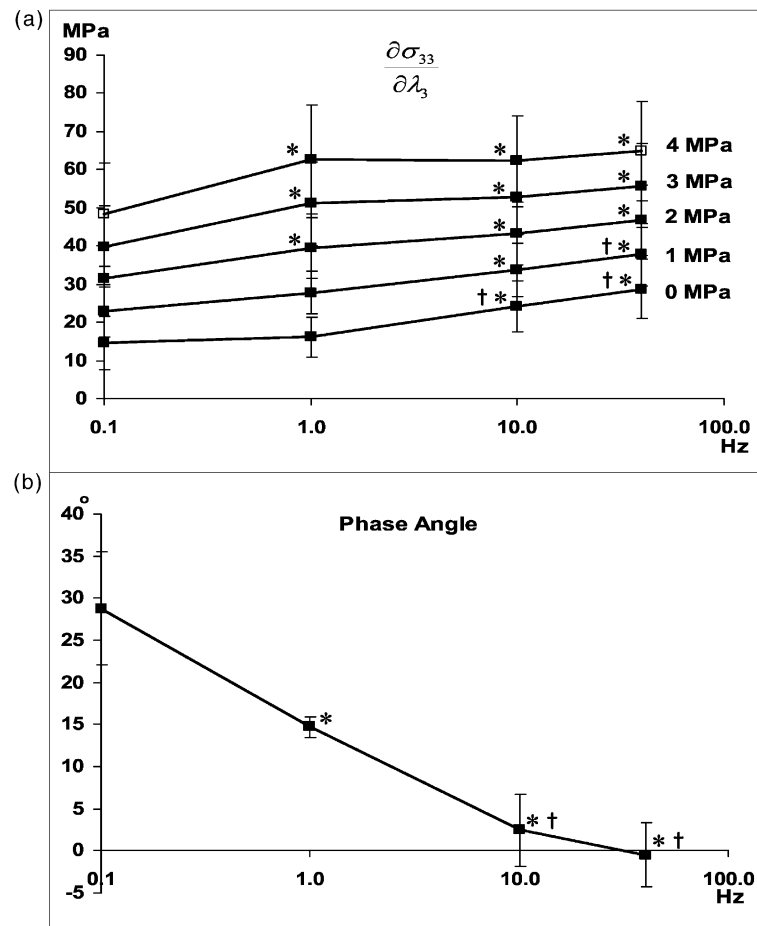


Fig. 4. (a) Mean and standard deviation of the incremental dynamic modulus ($\partial\sigma_{33}/\partial\lambda_3$) at selected values of the applied compressive stress σ_{33} , as a function of frequency. Open squares indicate data extrapolated from the experimental range, using the curve fits and coefficients of Table II. (b) Mean and standard deviation of the phase angle determined from the energy dissipation analysis over an entire loading cycle, as a function of frequency. Symbols denote significant statistical difference against corresponding values at 0.1 Hz (*) and at 1 Hz (†) ($P < 0.03$).

moduli are indicated in the figure. The phase angle derived from the area under the hysteresis loop of the stress vs strain response is shown in Fig. 4(b). A one-way ANOVA for the factor of loading frequency indicates significant differences as shown in the figure.

Discussion

The objective of this study was to characterize the mechanical response of bovine articular cartilage under physiological loading conditions (i.e., physiological load magnitudes and frequencies). Experimentally, this could be achieved using a load-control apparatus which can overcome loading platen lift-off artifacts that would otherwise occur under displacement-control at the high dynamic compressive strains achieved in this study. The range of loading frequencies employed here may be considered representative of activities of daily living and the magnitudes of applied stresses are in the range of light to moderate physical activities. The higher range of loading frequencies (10–40 Hz) approaches the range of traumatic impact loading, which occurs over durations of 5–50 ms⁴³, corresponding to the characteristic loading frequencies of

20–200 Hz. To our knowledge, this represents one of the broader ranges of conditions employed in unconfined compression testing of articular cartilage.

The state of stress and strain in contacting articular layers is complex, as estimated from contact analyses which assume various constitutive relations for cartilage^{12,44–47}. The unconfined compression testing configuration, with the bony substrate removed as performed in this study, does not necessarily capture the full complexity of cartilage response to contact loading *in situ*; however, because it subjects cartilage to compression in the axial direction (normal to the articular surface) and tension in the lateral (radial and circumferential) direction, it is more representative of *in situ* contact conditions than confined compression (which does not produce any tensile strains) or indentation with a porous-permeable filter, both of which allow tissue compaction at the interface with the filter, contrary to predictions from contact analyses where the porous-permeable nature of cartilage is taken into account. Indeed, as shown in our recent finite element study⁴⁸, the following analogies exist between physiological contact loading and unconfined compression: (a) the interstitial fluid pressurization is nearly uniform through the depth and interstitial fluid flow is predominantly in the direction

tangential to the articular surface under the contact region; (b) there is no compaction boundary layer at the articular surface in the loaded region; (c) the effective stresses (the stresses contributed by the strain in the solid matrix) are tensile in the direction tangential to the articular surface and compressive normal to the articular surface radial direction. Thus, the results of this study (as well as previous investigations of the dynamic modulus of cartilage in unconfined compression, e.g., references 18,21,41) can provide significant insight into the physiological loading environment of articular cartilage *in situ*.

The frequency dependence of the magnitude and phase angle of the dynamic modulus reported in Figs. 2 and 4 confirms the viscoelastic nature of articular cartilage in compression. Based on Fig. 4, it can be noted that the dynamic modulus of cartilage increases by up to a factor of 2 over the range of physiological loading frequencies due to its viscoelasticity. This experiment was not designed to distinguish between fluid flow-dependent and fluid flow-independent viscoelasticity of articular cartilage⁴⁹, as both effects are expected to be present in the loading configuration of unconfined compression^{38,50,51}. However, our recent theoretical studies suggest that flow-dependent viscoelasticity is less significant than flow-independent viscoelasticity at higher frequencies³⁸. That the phase angle reduces to zero at 40 Hz suggests that above this frequency cartilage behaves effectively as an elastic solid and that no further increase in dynamic modulus is to be expected. The dynamic modulus at various applied stresses similarly shows an increasing trend up until 40 Hz, statistically significant in most cases; the phase angle data suggest that the modulus should remain constant at higher frequencies. This is also evident from the typical stress–strain responses for a single cycle of loading displayed in Fig. 3 for each of the loading frequencies. A larger hysteresis loop is evident at the lower frequencies, indicative of energy dissipation over that loading cycle. At the higher frequencies however, the hysteresis loop diminishes in area and is eliminated at 40 Hz. Note that this result is somewhat different from that of Kim *et al.*²⁰ who found that the phase angle reduces nearly to zero at 1 Hz, for similarly sized bovine cartilage specimens. One potential explanation for this difference is that the loading in the current study produced significantly higher compressive strains that may lead to greater energy dissipation from flow-dependent or flow-independent effects. Another potential reason is the difference in the methods of analysis, since the short-term nonlinear stress–strain response observed in this study precluded the use of Fourier analysis, commonly employed to extract the dynamic modulus from steady-state sinusoidal data in small strain studies^{18,21,41}. It is interesting that the nearly elastic behavior reported here occurs in the upper range of physiological loading frequencies, which may serve as an important insight in studies of the biosynthetic response and viability of chondrocytes under various loading frequencies and impact rates^{21,43,52–55}. At lower loading frequencies, cartilage dissipates a fraction of the energy imparted by loading through viscous dissipation, storing only some of the energy in the form of recoverable elastic strain in the solid matrix; with increasing loading frequency (or rate of loading) however, the tissue increasingly stores the energy input in the form of elastic strain. The failure characteristics of cartilage at various loading frequencies are not addressed in the current study, but are related to limits in its capacity to store energy. It should be kept in perspective however, that the characteristic frequency response of a

biphasic material in unconfined compression is inversely dependent on the square of the radius. According to theory, the frequency response shown in Fig. 4 would therefore shift to the left for larger tissue samples, decreasing the energy dissipation at a given frequency²³.

Another important result is the observation of significant nonlinearity in the stress–strain response under physiological compressive stresses (Figs. 3 and 4, Table II). For example, at 1 Hz, the slope of the stress–strain curve at zero stress and strain averages ~16 MPa; at approximately 4.8 MPa and 13% compression (Table I) it increases to ~66 MPa (Table II). The results of Fig. 4 also clearly indicate that with increasing applied stress amplitude, the dynamic modulus correspondingly increases. The peak dynamic moduli reported in this study, where the applied stresses are in the physiological range, are significantly greater than those reported to date as reviewed in the Introduction (e.g., 13–37 MPa). This finding goes a long way to explain why cartilage is able to sustain the physiological stresses predicted from joint contact studies without crushing the articular layer. Even at the lowest reported frequency of 0.1 Hz, the compressive strain is only 16% with ~4 MPa (true) compressive stress; at 40 Hz, it decreases to 9% (Table I). Using the curve-fitted coefficients provided in Table II, it is possible to get an educated estimate of the magnitude of compressive strains at even higher compressive stresses by extrapolation. For example, with 12 MPa of dynamic compression at 1 Hz, the compressive strain amplitude would be ~18% while the peak dynamic modulus at that strain would be ~158 MPa. The nonlinear response clearly reduces the increase in strain with increasing stress. Due to the viscoelastic nature of the tissue, the compressive strain magnitudes will be smaller at higher loading frequencies, under the same compressive stresses. Furthermore, the peak compressive stresses predicted in the literature are likely to occur at higher loading rates (e.g., ≥ 1 Hz), suggesting that compressive strains of 20% may be typical under normal physiological conditions. It is important to note however, that higher contact stresses would produce higher compressive strains, and that compressive strain magnitudes may depend on age, as cartilage from immature joints is known to have lower moduli than adult tissue⁵⁶. The nonlinearity observed in this study extends the recent findings of Fortin *et al.*²³ to the range of physiological stress magnitudes; however, those authors noted a decrease in dynamic stiffness with increasing displacement amplitude in a displacement-control study, which is not supported by the current findings.

Recent theoretical developments have led to the hypothesis that the dynamic modulus of articular cartilage in unconfined compression is significantly dependent on interstitial fluid pressurization and the tensile properties of the collagen–proteoglycan extracellular matrix^{38,57–60}, because axial compression of the tissue produces tensile strains in the radial and circumferential directions. In our recent study, it was predicted that the dynamic unconfined compression modulus is approximately proportional to half of the tensile modulus (Eq. (16) of reference 38). Since the tensile modulus of cartilage at various loading rates has been shown to be approximately in the range of 20–150 MPa^{61–63}, the results of the current study are consistent with the model predictions and strongly support the hypothesis that tensile properties of cartilage significantly regulate the dynamic properties in compression. The nonlinear stiffening of collagen fibrils in tension was explicitly modeled by Li *et al.*⁶⁴ to describe the response of

cartilage in unconfined compression and the results of our study strongly support this modeling assumption. The relationship between the dynamic modulus in compression and the tensile modulus of the matrix yields important insight into the mechanics of cartilage because it suggests that any degradative process which compromises the tensile properties (as evidenced for example, by articular surface fibrillation) will have a detrimental effect on the dynamic compressive properties as well.

Both viscoelasticity and nonlinearity play an important role in providing cartilage the functional properties that allow it to sustain the loading environment in joints. The fact that the equilibrium compressive modulus, at ~ 0.5 MPa, is so much lower than the dynamic moduli at physiological loading frequencies suggests that equilibrium properties alone are not sufficiently representative of the functional response of this tissue. This is especially relevant in tissue engineering studies of articular cartilage which aim to achieve a functional tissue substitute^{65,66}. While many investigators, including ourselves, have used the equilibrium confined or unconfined compression modulus of tissue constructs as a measure of matrix elaboration^{31,67,68}, the current findings emphasize that it is also important to report the dynamic unconfined compression modulus as it may be more representative of tissue function. Knowing the magnitude of physiological compressive strains is also useful for regulating the loading environment of engineered tissue constructs³¹. Based on this study, we estimate that compressive strains in the range of 10–20% fall within the normal physiological range, which is consistent with previous literature studies which have addressed this question with alternative methodologies^{11–14}.

While new information on the behavior of articular cartilage under physiologic loading is provided by our analyses, it is important to outline the potential limitations of this study. The cartilage samples were not bonded to bone; it is generally expected that a bony substrate would stiffen the structural response by limiting the lateral expansion of the tissue in the deep zone, which in turn may result in smaller compressive strains. Conversely, it is more difficult to extract intrinsic material properties from a test where the cartilage is bonded to bone, whereas the data from the current study may be used to determine such properties, within an appropriately defined finite deformation theory. In the analysis of the results, it was assumed that the tissue is homogeneous through the depth, whereas it is well established that the mechanical properties of cartilage are depth-dependent. The results of this study should be interpreted as depth-averaged properties of the articular layer. In immature cartilage it is also more difficult to determine the exact interface between cartilage and bone; specimens were microtomed to remove gross evidence of vascularization, which may have influenced the measurements of this study. Finally, this study analyzes the short-time response of the tissue, over a few seconds of loading, and it may be interesting to extend this type of analysis to longer term dynamic loading, over an hour or more.

Since chondrocytes undergo depth-varying deformation in loaded explants⁶⁹, which may be attributed to the disparate material properties through the tissue depth^{69,70} and/or to differences in properties of chondrocytes in the varying zones⁷¹, the inhomogeneity of the tissue will need to be considered when attempting to identify the underlying mechanisms that mediate chondrocyte mechanotransduction⁷². Moreover, the presence of the stiffer pericellular matrix of the chondron⁷³, contributing to the local cell milieu, will further influence the level of extracellular matrix

deformation experienced by the chondrocyte^{74,75}. For the purpose of analyzing the results in the proper context of finite deformation theory, it was also assumed that the tissue response was incompressible. This assumption is believed to be substantially satisfied at the higher loading frequencies based on the intrinsic incompressibility of the tissue^{76,77} and minimal fluid flow, as demonstrated from our recent theoretical study which shows negligible flow-dependent effects above 0.1 Hz (Fig. 4 of reference 38). It was also assumed that the loading platens are frictionless, which is reasonable in the light of low friction coefficient of cartilage under dynamic loading conditions that promote elevated interstitial fluid pressurization. While the amplitude of the applied load could be controlled in this study, the amplitude of the true stress could not be maintained constant across all specimens because the true contact area varied with loading and was specimen-specific. Finally, this experimental study did not propose any constitutive model of cartilage based on the data; a simple curve-fitting function was employed here to smooth the stress–strain response and to calculate its slope. In future theoretical studies, we expect to employ these experimental results to formulate a finite deformation constitutive relation, which accounts for the observed nonlinear responses, as well as the flow-dependent and flow-independent viscoelasticity and interstitial fluid pressurization of cartilage.

Acknowledgements

This study was supported by funds from the National Institute of Arthritis and Musculoskeletal and Skin Diseases of the National Institutes of Health (AR-46532, AR-43628).

References

1. Cooney WP, Chao EYS. Biomechanical analysis of static forces in the thumb during hand functions. *J Bone Joint Surg Am* 1977;59:27–36.
2. Paul JP. Forces transmitted by joints in the human body. *Proc Inst Mech Eng* 1967;181(3J):8.
3. Poppen NK, Walker PS. Forces at the glenohumeral joint in abduction. *Clin Orthop* 1978;135:165–70.
4. Rydell N. Forces in the hip joint: part (II) Intra-vital measurements. In: Kenedi RM, Ed. *Biomechanics and Related Bio-Engineering Topics*. Oxford: Pergamon Press 1965.
5. Ahmed AM, Burke DL. In-vitro measurement of static pressure distribution in synovial joints—part I: tibial surface of the knee. *J Biomech Eng* 1983;105: 216–25.
6. Brown TD, Shaw DT. In vitro contact stress distributions in the natural human hip. *J Biomech* 1983; 16:373–84.
7. Huberti HH, Hayes WC. Patellofemoral contact pressures. *J Bone Joint Surg Am* 1984;66:715–24.
8. Hodge WA, Carlson KL, Fijan RS, Burgess RG, Riley PO, Harris WH, *et al.* Contact pressures from an instrumented hip endoprosthesis. *J Bone Joint Surg Am* 1989;71:1378–86.
9. Matthews LS, Sonstegard DA, Hanke JA. Load bearing characteristics of the patello-femoral joint. *Acta Orthop Scand* 1977;48:511–6.
10. Clark AL, Herzog W, Leonard TR. Contact area and pressure distribution in the feline patellofemoral joint

- under physiologically meaningful loading conditions. *J Biomech* 2002;35:53–60.
11. Armstrong CG, Bahrani AS, Gardner DL. In vitro measurement of articular cartilage deformations in the intact human hip joint under load. *J Bone Joint Surg Am* 1979;61:744–55.
 12. Macirowski T, Tepic S, Mann RW. Cartilage stresses in the human hip joint. *J Biomech Eng* 1994;116:10–8.
 13. Eckstein F, Lemberger B, Stammberger T, Englmeier KH, Reiser M. Patellar cartilage deformation in vivo after static versus dynamic loading. *J Biomech* 2000;33:819–25.
 14. Eckstein F, Tieschky M, Faber S, Englmeier K-H, Reiser M. Functional analysis of articular cartilage deformation, recovery, and fluid flow following dynamic exercise *in vivo*. *Anat Embryol* 1999;200:419–24.
 15. Herberhold C, Faber S, Stammberger T, Steinlechner M, Putz R, Englmeier K-H, *et al.* *In situ* measurement of articular cartilage deformation in intact femoropatellar joints under static loading. *J Biomech* 1999;32:1287–95.
 16. Kaab MJ, Ito K, Clark JM, Notzli HP. Deformation of articular cartilage collagen structure under static and cyclic loading. *J Orthop Res* 1998;16:743–51.
 17. Bonassar LJ, Grodzinsky AJ, Frank EH, Davila SG, Bhaktav NR, Trippel SB. The effect of dynamic compression on the response of articular cartilage to insulin-like growth factor-I. *J Orthop Res* 2001;19:11–7.
 18. Buschmann MD, Kim YJ, Wong M, Frank E, Hunziker EB, Grodzinsky AJ. Stimulation of aggrecan synthesis in cartilage explants by cyclic loading is localized to regions of high interstitial fluid flow. *Arch Biochem Biophys* 1999;366:1–7.
 19. Guilak F, Meyer BC, Ratcliffe A, Mow VC. The effects of matrix compression on proteoglycan metabolism in articular cartilage explants. *Osteoarthritis Cartilage* 1994;2:91–101.
 20. Kim YJ, Bonassar LJ, Grodzinsky AJ. The role of cartilage streaming potential, fluid flow and pressure in the stimulation of chondrocyte biosynthesis during dynamic compression. *J Biomech* 1995;28:1055–66.
 21. Sah RL, Kim YJ, Doong JY, Grodzinsky AJ, Plaas AH, Sandy JD. Biosynthetic response of cartilage explants to dynamic compression. *J Orthop Res* 1989;7:619–36.
 22. Wong M, Wuethrich P, Buschmann MD, Egli P, Hunziker E. Chondrocyte biosynthesis correlates with local tissue strain in statically compressed adult articular cartilage. *J Orthop Res* 1997;15:189–96.
 23. Fortin M, Soulhat J, Shirazi-Adl A, Hunziker EB, Buschmann MD. Unconfined compression of articular cartilage: nonlinear behavior and comparison with a fibril-reinforced biphasic model. *J Biomed Eng* 2000;122:189–95.
 24. Buschmann MD, Gluzband YA, Grodzinsky AJ, Hunziker EB. Mechanical compression modulates matrix biosynthesis in chondrocyte/agarose culture. *J Cell Sci* 1995;108:1497–508.
 25. Elder SH, Goldstein SA, Kimura JH, Soslowky LJ, Spengler DM. Chondrocyte differentiation is modulated by frequency and duration of cyclic compressive loading. *Ann Biomed Eng* 2001;29:476–82.
 26. Knight MM, van de Breevaart Bravenboer J, Lee DA, van Osch GJ, Weinans H, Bader DL. Cell and nucleus deformation in compressed chondrocyte–alginate constructs: temporal changes and calculation of cell modulus. *Biochim Biophys Acta* 2002;1570:1–8.
 27. Lee DA, Bader DL. Compressive strains at physiological frequencies influence the metabolism of chondrocytes seeded in agarose. *J Orthop Res* 1997;15:181–8.
 28. Freed LE, Martin I, Vunjak-Novakovic G. Frontiers in tissue engineering. In vitro modulation of chondrogenesis. *Clin Orthop* 1999;367:S46–S58.
 29. Gooch KJ, Blunk T, Courter DL, Sieminski AL, Bursac PM, Vunjak-Novakovic G, *et al.* IGF-I and mechanical environment interact to modulate engineered cartilage development. *Biochem Biophys Res Commun* 2001;286:909–15.
 30. Li KW, Falcovitz YH, Nagrampa JP, Chen AC, Lottman LM, Shyy JY, *et al.* Mechanical compression modulates proliferation of transplanted chondrocytes. *J Orthop Res* 2000;18:374–82.
 31. Mauck RL, Soltz MA, Wang CC, Wong DD, Chao PH, Valhmu WB, *et al.* Functional tissue engineering of articular cartilage through dynamic loading of chondrocyte-seeded agarose gels. *J Biomech Eng* 2000;122:252–60.
 32. Vunjak-Novakovic G, Obradovic B, Martin I, Freed LE. Bioreactor studies of native and tissue engineered cartilage. *Biorheology* 2002;39:259–68.
 33. Armstrong CG, Mow VC. Variations in the intrinsic mechanical properties of human articular cartilage with age, degeneration, and water content. *J Bone Joint Surg Am* 1982;64:88–94.
 34. Ateshian GA, Warden WH, Kim JJ, Grelsamer RP, Mow VC. Finite deformation biphasic material properties of bovine articular cartilage from confined compression experiments. *J Biomech* 1997;30:1157–64.
 35. Mow VC, Kuei SC, Lai WM, Armstrong CG. Biphasic creep and stress relaxation of articular cartilage in compression? Theory and experiments. *J Biomech Eng* 1980;102:73–84.
 36. Soltz MA, Ateshian GA. Experimental verification and theoretical prediction of cartilage interstitial fluid pressurization at an impermeable contact interface in confined compression. *J Biomech* 1998;31:927–34.
 37. Zarek JM, Edwards J. A note on the stress–structure relationship in articular cartilage. *Med Electron Biol Eng* 1965;3:449–50.
 38. Huang CY, Mow VC, Ateshian GA. The role of flow-independent viscoelasticity in the biphasic tensile and compressive responses of articular cartilage. *J Biomech Eng* 2001;123:410–7.
 39. Lee RC, Frank EH, Grodzinsky AJ, Roylance DK. Oscillatory compressional behavior of articular cartilage and its associated electromechanical properties. *J Biomech Eng* 1981;103:280–92.
 40. Soltz MA, Ateshian GA. Interstitial fluid pressurization during confined compression cyclical loading of articular cartilage. *Ann Biomed Eng* 2000;28:150–9.
 41. Kim YJ, Bonassar LJ, Grodzinsky AJ. The role of cartilage streaming potential, fluid flow and pressure in the stimulation of chondrocyte biosynthesis during dynamic compression. *J Biomech* 1995;28:1055–66.
 42. Lai WM, Rubin D, Kreml E. *Introduction to Continuum Mechanics*, 3rd edn. Oxford: Pergamon Press 1993;203–7.
 43. Ewers BJ, Jayaraman VM, Banglmaier RF, Haut RC. Rate of blunt impact loading affects changes in

- retropatellar cartilage and underlying bone in the rabbit patella. *J Biomech* 2002;35:747–55.
44. Ateshian GA, Lai WM, Zhu WB, Mow VC. An asymptotic solution for the contact of two biphasic cartilage layers. *J Biomech* 1994;27:1347–60.
 45. Donzelli PS, Spilker RL, Ateshian GA, Mow VC. Contact analysis of biphasic transversely isotropic cartilage layers and correlations with tissue failure. *J Biomech* 1999;32:1037–47.
 46. Eberhardt AW, Lewis JL, Keer LM. Normal contact of elastic spheres with two elastic layers as a model of joint articulation. *J Biomech Eng* 1991;113:410–7.
 47. Garcia JJ, Altiero NJ, Haut RC. An approach for the stress analysis of transversely isotropic biphasic cartilage under impact load. *J Biomech Eng* 1998;120:608–13.
 48. Park S, Krishnan R, Nicoll SB, Ateshian GA. Cartilage interstitial fluid load support in unconfined compression. *J Biomech* 2003;36:1785–96.
 49. Mak AF. The apparent viscoelastic behavior of articular cartilage—the contributions from the intrinsic matrix viscoelasticity and interstitial fluid flows. *J Biomech Eng* 1986;108:123–30.
 50. DiSilvestro MR, Zhu Q, Suh JK. Biphasic poroviscoelastic simulation of the unconfined compression of articular cartilage: II—effect of variable strain rates. *J Biomech Eng* 2001;123:198–200.
 51. Mak AF. Unconfined compression of hydrated viscoelastic tissues: a biphasic poroviscoelastic analysis. *Biorheology* 1986;23:371–83.
 52. Chen CT, Burton-Wurster N, Borden C, Hueffer K, Bloom SE, Lust G. Chondrocyte necrosis and apoptosis in impact damaged articular cartilage. *J Orthop Res* 2001;19:703–11.
 53. Duda GN, Eilers M, Loh L, Hoffman JE, Kaab M, Schaser K. Chondrocyte death precedes structural damage in blunt impact trauma. *Clin Orthop* 2001;393:302–9.
 54. Jeffrey JE, Gregory DW, Aspden RM. Matrix damage and chondrocyte viability following a single impact load on articular cartilage. *Arch Biochem Biophys* 1995;322:87–96.
 55. Torzilli PA, Grigiene R, Borrelli J Jr, Helfet DL. Effect of impact load on articular cartilage: cell metabolism and viability, and matrix water content. *J Biomech Eng* 1999;121:433–41.
 56. Williamson AK, Chen AC, Sah RL. Compressive properties and function–composition relationships of developing bovine articular cartilage. *J Orthop Res* 2001;19:1113–21.
 57. Cohen B, Lai WM, Mow VC. A transversely isotropic biphasic model for unconfined compression of growth plate and chondroepiphysis. *J Biomech Eng* 1998;120:491–6.
 58. Mizrahi J, Maroudas A, Lanir Y, Ziv I, Webber TJ. The “instantaneous” deformation of cartilage: effects of collagen fiber orientation and osmotic stress. *Biorheology* 1986;23:311–30.
 59. Soltz MA, Ateshian GA. A conewise linear elasticity mixture model for the analysis of tension–compression nonlinearity in articular cartilage. *J Biomech Eng* 2000;122:576–86.
 60. Soulhat J, Buschmann MD, Shirazi-Adl A. A fibril-network-reinforced biphasic model of cartilage in unconfined compression. *J Biomech Eng* 1999;121:340–7.
 61. Akizuki S, Mow VC, Muller F, Pita JC, Howell DS, Manicourt DH. Tensile properties of human knee joint cartilage: I. Influence of ionic conditions, weight bearing, and fibrillation on the tensile modulus. *J Orthop Res* 1986;4:379–92.
 62. Kempson GE. Mechanical properties of articular cartilage. In: Freeman MAR, Ed. *Adult Articular Cartilage*, 2nd edn. Kent, England: Pitman Medical 1979.
 63. Woo SL, Lubock P, Gomez MA, Jemmott GF, Kuei SC, Akeson WH. Large deformation nonhomogeneous and directional properties of articular cartilage in uniaxial tension. *J Biomech* 1979;12:437–46.
 64. Li LP, Soulhat J, Buschmann MD, Shirazi-Adl A. Non-linear analysis of cartilage in unconfined ramp compression using a fibril reinforced poroelastic model. *Clin Biomech* 1999;14:673–82.
 65. Butler DL, Goldstein SA, Guilak F. Functional tissue engineering: the role of biomechanics. *J Biomech Eng* 2000;122:570–5.
 66. Guilak F, Butler DL, Goldstein SA. Functional tissue engineering: the role of biomechanics in articular cartilage repair. *Clin Orthop* 2001;391:S295–S305.
 67. Carver SE, Heath CA. Influence of intermittent pressure, fluid flow, and mixing on the regenerative properties of articular chondrocytes. *Biotechnol Bioeng* 1999;65:274–81.
 68. Vunjak-Novakovic G, Martin I, Obradovic B, Treppo S, Grodzinsky AJ, Langer R, *et al.* Bioreactor cultivation conditions modulate the composition and mechanical properties of tissue-engineered cartilage. *J Orthop Res* 1999;17:130–8.
 69. Guilak F, Ratcliffe A, Mow VC. Chondrocyte deformation and local tissue strain in articular cartilage: a confocal microscopy study. *J Orthop Res* 1995;13:410–22.
 70. Schinagl RM, Gurkis D, Chen CC, Sah RL. Depth-dependent confined compression modulus of full-thickness bovine articular cartilage. *J Orthop Res* 1997;15:499–506.
 71. Lee DA, Bader DL. The development and characterization of an in vitro system to study strain-induced cell deformation in isolated chondrocytes. *In Vitro Cell Dev Biol Anim* 1995;31:828–35.
 72. Wang CC-B, Guo XE, Sun D, Mow VC, Ateshian GA, Hung CT. The functional environment of chondrocytes within cartilage subjected to compressive loading: theoretical and experimental approach. *Biorheology* 2002;39:39–45.
 73. Guilak F, Jones WR, Ting-Beall HP, Lee GM. The deformation behavior and mechanical properties of chondrocytes in articular cartilage. *Osteoarthritis Cartilage* 1999;7:59–70.
 74. Knight MM, Ross JM, Sherwin AF, Lee DA, Bader DL, Poole CA. Chondrocyte deformation within mechanically and enzymatically extracted chondrons compressed in agarose. *Biochim Biophys Acta* 2001;1526:141–6.
 75. Poole CA. Articular cartilage chondrons: form, function and failure. *J Anat* 1997;191:1–13.
 76. Bachrach NM, Mow VC, Guilak F. Incompressibility of the solid matrix of articular cartilage under high hydrostatic pressures. *J Biomech* 1998;31:445–51.
 77. Wong M, Ponticello M, Kovanen V, Jurvelin JS. Volumetric changes of articular cartilage during stress relaxation in unconfined compression. *J Biomech* 2000;33:1049–54.